Research Article | Vol. 7, No. 9 | 1 Sept 2016 | BIOMEDICAL OPTICS EXPRESS 3220
Biomedical Optics EXPRESS

Visible-light optical coherence tomography-based multimodal retinal imaging for improvement of fluorescent intensity quantification

ZAHRA NAFAR,[1] MINSHAN JIANG,[1] RONG WEN,[2] AND SHULIANG JIAO,[1,*]

[1]*Department of Biomedical Engineering, Florida International University, 10555 W Flagler ST, EC-2610, Miami, FL 33174, USA*
[2]*Bascom Palmer Eye Institute, University of Miami Miller School of Medicine, 1638 NW 10 Ave, Miami, FL 33136, USA*
**shjiao@fiu.edu*

Abstract: We developed a spectral-domain visible-light optical coherence tomography (VIS-OCT) based multimodal imaging technique which can accomplish simultaneous OCT and fluorescence imaging with a single broadband light source. Phantom experiments showed that by using the simultaneously acquired OCT images as a reference, the effect of light attenuation on the intensity of the fluorescent images by materials in front of the fluorescent target can be compensated. This capability of the multimodal imaging technique is of high importance for achieving quantification of the true intensities of autofluorescence (AF) imaging of the retina. We applied the technique in retinal imaging including AF imaging of the retinal pigment epithelium and fluorescein angiography (FA). We successfully demonstrated the effect of compensation on AF and FA images with the simultaneously acquired VIS-OCT images.

OCIS codes: (170.3880) Medical and biological imaging; (110.4500) Optical coherence tomography; (170.2520) Fluorescence microscopy; (170.4470) Ophthalmology; (170.4580) Optical diagnostics for medicine.

References and links

1. D. Huang, E. A. Swanson, C. P. Lin, J. S. Schuman, W. G. Stinson, W. Chang, M. R. Hee, T. Flotte, K. Gregory, C. A. Puliafito, and et, "Optical coherence tomography," Science **254**(5035), 1178–1181 (1991).
2. M. Wojtkowski, V. Srinivasan, T. Ko, J. Fujimoto, A. Kowalczyk, and J. Duker, "Ultrahigh-resolution, high-speed, Fourier domain optical coherence tomography and methods for dispersion compensation," Opt. Express **12**(11), 2404–2422 (2004).
3. A. D. Singh, R. N. Belfort, K. Sayanagi, and P. K. Kaiser, "Fourier domain optical coherence tomographic and auto-fluorescence findings in indeterminate choroidal melanocytic lesions," Br. J. Ophthalmol. **94**(4), 474–478 (2010).
4. F. C. Delori, C. K. Dorey, G. Staurenghi, O. Arend, D. G. Goger, and J. J. Weiter, "In vivo fluorescence of the ocular fundus exhibits retinal pigment epithelium lipofuscin characteristics," Invest. Ophthalmol. Vis. Sci. **36**(3), 718–729 (1995).
5. G. De Venecia, M. Davis, and R. Engerman, "Clinicopathologic correlations in diabetic retinopathy. i. histology and fluorescein angiography of microaneurysms," Arch. Ophthalmol. **94**(10), 1766–1773 (1976).
6. F. G. Holz, C. Bellmann, K. Rohrschneider, R. O. W. Burk, and H. E. Völcker, "Simultaneous confocal scanning laser fluorescein and indocyanine green angiography," Am. J. Ophthalmol. **125**(2), 227–236 (1998).
7. M. Boulton, N. M. McKechnie, J. Breda, M. Bayly, and J. Marshall, "The formation of autofluorescent granules in cultured human RPE," Invest. Ophthalmol. Vis. Sci. **30**(1), 82–89 (1989).
8. J. R. Sparrow and M. Boulton, "RPE lipofuscin and its role in retinal pathobiology," Exp. Eye Res. **80**(5), 595–606 (2005).
9. E. J. Johnson, "Age-related macular degeneration and antioxidant vitamins: recent findings," Curr. Opin. Clin. Nutr. Metab. Care **13**(1), 28–33 (2010).
10. B. Povazay, A. A. Apolonski, A. Unterhuber, B. Hermann, K. K. Bizheva, H. Sattmann, P. S. J. Russell, F. Krausz, A. F. Fercher, and W. Drexler, "Visible light optical coherence tomography," Proc. SPIE **4619**, 90–94 (2002).
11. X. Zhang, J. Hu, R. W. Knighton, X.-R. Huang, C. A. Puliafito, and S. Jiao, "Dual-band spectral-domain optical coherence tomography for in vivo imaging the spectral contrasts of the retinal nerve fiber layer," Opt. Express **19**(20), 19653–19659 (2011).

#268335 http://dx.doi.org/10.1364/BOE.7.003220
Journal © 2016 Received 14 Jun 2016; revised 31 Jul 2016; accepted 31 Jul 2016; published 4 Aug 2016

Biomedical Optics EXPRESS

12. C. Dai, X. Liu, and S. Jiao, "Simultaneous optical coherence tomography and autofluorescence microscopy with a single light source," J. Biomed. Opt. **17**(8), 080502 (2012).
13. M. Jiang, T. Liu, X. Liu, and S. Jiao, "Simultaneous optical coherence tomography and lipofuscin autofluorescence imaging of the retina with a single broadband light source at 480nm," Biomed. Opt. Express **5**(12), 4242–4248 (2014).
14. J. Yi, Q. Wei, W. Liu, V. Backman, and H. F. Zhang, "Visible-light optical coherence tomography for retinal oximetry," Opt. Lett. **38**(11), 1796–1798 (2013).
15. F. Delori, J. P. Greenberg, R. L. Woods, J. Fischer, T. Duncker, J. Sparrow, and R. T. Smith, "Quantitative measurements of autofluorescence with the scanning laser ophthalmoscope," Invest. Ophthalmol. Vis. Sci. **52**(13), 9379–9390 (2011).
16. J. Pokorny, V. C. Smith, and M. Lutze, "Aging of the human lens," Appl. Opt. **26**(8), 1437–1440 (1987).
17. C. Dai, X. Liu, H. F. Zhang, C. A. Puliafito, and S. Jiao, "Absolute retinal blood flow measurement with a dual-beam Doppler optical coherence tomography," Invest. Ophthalmol. Vis. Sci. **54**(13), 7998–8003 (2013).
18. J. van de Kraats, T. T. Berendschot, and D. van Norren, "The pathways of light measured in fundus reflectometry," Vision Res. **36**(15), 2229–2247 (1996).
19. J. I. W. Morgan and E. N. Pugh, Jr., "Scanning Laser Ophthalmoscope Measurement of Local Fundus Reflectance and Autofluorescence Changes Arising from Rhodopsin Bleaching and Regeneration," Invest. Ophthalmol. Vis. Sci. **54**(3), 2048–2059 (2013).
20. S. Jiao, R. Knighton, X. Huang, G. Gregori, and C. Puliafito, "Simultaneous acquisition of sectional and fundus ophthalmic images with spectral-domain optical coherence tomography," Opt. Express **13**(2), 444–452 (2005).
21. F. C. Delori, G. Staurenghi, O. Arend, C. K. Dorey, D. G. Goger, and J. J. Weiter, "In vivo measurement of lipofuscin in Stargardt's disease--Fundus flavimaculatus," Invest. Ophthalmol. Vis. Sci. **36**(11), 2327–2331 (1995).
22. F. C. Delori, S. E. Bursell, A. Yoshida, and J. W. McMeel, "Vitreous fluorophotometry in diabetics: study of artifactual contributions," Graefes Arch. Clin. Exp. Ophthalmol. **222**(4-5), 215–218 (1985).
23. J. R. Sparrow, N. Fishkin, J. Zhou, B. Cai, Y. P. Jang, S. Krane, Y. Itagaki, and K. Nakanishi, "A2E, a byproduct of the visual cycle," Vision Res. **43**(28), 2983–2990 (2003).
24. J. R. Sparrow, E. Gregory-Roberts, K. Yamamoto, A. Blonska, S. K. Ghosh, K. Ueda, and J. Zhou, "The bisretinoids of retinal pigment epithelium," Prog. Retin. Eye Res. **31**(2), 121–135 (2012).
25. J. R. Sparrow and M. Boulton, "RPE lipofuscin and its role in retinal pathobiology," Exp. Eye Res. **80**(5), 595–606 (2005).
26. O. Strauss, "The retinal pigment epithelium in visual function," Physiol. Rev. **85**(3), 845–881 (2005).
27. P. D. Kiser, M. Golczak, and K. Palczewski, "Chemistry of the retinoid (visual) cycle," Chem. Rev. **114**(1), 194–232 (2014).
28. B. M. Kevany and K. Palczewski, "Phagocytosis of retinal rod and cone photoreceptors," Physiology (Bethesda) **25**(1), 8–15 (2010).
29. X. Zhang, H. F. Zhang, C. A. Puliafito, and S. Jiao, "Simultaneous in vivo imaging of melanin and lipofuscin in the retina with multimodal photoacoustic ophthalmoscopy," J. Biomed. Opt. **16**, 080504 (2011).
30. X. Zhang, M. Jiang, A. A. Fawzi, X. Li, K. K. Shung, C. A. Puliafito, H. F. Zhang, and S. Jiao, "Simultaneous dual molecular contrasts provided by the absorbed photons in photoacoustic microscopy," Opt. Lett. **35**(23), 4018–4020 (2010).
31. X. Zhang, H. F. Zhang, S. Jiao, and S. Jiao, "Optical Coherence Photoacoustic Microscopy: accomplishing optical coherence tomography and photoacoustic microscopy with a single light source," J. Biomed. Opt. **17**(3), 030502 (2012).
32. X. Liu, T. Liu, R. Wen, Y. Li, C. A. Puliafito, H. F. Zhang, and S. Jiao, "Optical coherence photoacoustic microscopy for in vivo multimodal retinal imaging," Opt. Lett. **40**(7), 1370–1373 (2015).
33. E. A. Boettner and J. R. Wolter, "Transmission of the ocular media," Invest. Ophthalmol. Vis. Sci. **1**(6), 776–783 (1962).
34. J. J. Weiter, F. C. Delori, G. L. Wing, and K. A. Fitch, "Retinal pigment epithelial lipofuscin and melanin and choroidal melanin in human eyes," Invest. Ophthalmol. Vis. Sci. **27**(2), 145–152 (1986).

1. Introduction

Optical coherence tomography (OCT) [1,2], retinal autofluorescence (AF) imaging [3,4], and fluorescein angiography (FA) [5,6] are three important imaging modalities in both ophthalmic clinics and research, which image different aspects of the retina. OCT is a low-coherence interferometry based imaging modality, which can provide mainly structural imaging of the retina with microscopic depth resolution. Retinal AF imaging maps the distribution of lipofuscin, the major source of AF in the retinal pigment epithelium (RPE). Lipofuscin is a complex lipid/protein aggregates formed in the RPE as nondegradable end products from phagocytosis of shed photoreceptor outer segments [7], which accumulate with age. Lipofuscin has influences on the RPE cells in many ways that are believed to contribute to the pathogenesis of age-related macular degeneration (AMD) [8,9]. FA images fluorescence from

Biomedical Optics EXPRESS

exogenous contrast molecules administrated into the blood stream to capture the blood circulations and identify vascular leakage in the retina. Because of the complementary nature of their contrast mechanisms, these imaging modalities are suitable candidates for being integrated into a multimodal imaging system. A broadband visible light source can be used to build such a multimodal imaging system, since retinal AF and FA needs visible light for fluorophore excitation. Visible light OCT (VIS-OCT) is gaining more attention in molecular contrast imaging recently because many molecules of interest in the retina have absorption spectra in the visible light range [10–14].

We recently achieved simultaneous OCT and AF imaging with a single broadband visible light source and successfully applied the imaging technique to monitor the accumulation of lipofuscin in the RPE cells in albino rats [12,13]. The current system was designed to compensate the signal attenuation by the media anterior to the RPE to tackle a technical difficulty in quantification of absolute AF intensities. Quantification of the absolute AF intensities is a major issue that the current retinal AF imaging technologies are not able to address [15]. During AF imaging, the excitation light must travel through the media anterior to the RPE before exciting the fluorophores, and the AF signals generated in the RPE must travel through the same media before being detected by the system. Signals are attenuated by these tissues, including the cornea, the aqueous humor, the vitreous, and especially by the lens [16].

The AF intensities changes in aging, as well as in certain pathological conditions, such as in AMD and Stargardt diseases. Monitoring AF changes would be informative for disease progression, for which quantitative accuracy is important to see the difference between individuals as well as longitudinal changes in the same eye. However, the measured AF in an image can be affected by many factors, including the optical properties of the anterior segments of the eye, which are different among different individuals and change over time; the intensity of the excitation light; and even alignment of the eye with the excitation light beam. Eliminating the influence of all the factors that are not related to the optical properties of the RPE would improve the quantification accuracy of AF imaging, which will make it possible to compare the overall AF intensities as well as changes in the spatial distribution of AF.

The current multimodal imaging system can simultaneously acquire OCT and AF imaging with a single broadband visible light source. Because the OCT signals are attenuated by the same media as the AF signals, the OCT signals can be used as an internal reference to compensate the signal attenuation by the media anterior to the RPE. Thus, our VIS-OCT based multimodal imaging technique offers a unique opportunity for compensation of the anterior segment attenuation effects on retinal AF imaging. This technique can also be used for retinal FA imaging. This paper reports our recent progress in simultaneous VIS-OCT, retinal AF, and FA imaging.

2. Methods

2.1 Imaging system

A schematic of the experimental system is shown in Fig. 1. The system has two SD-OCTs: one works in the NIR band (Fig. 1. red lines) and the other in the VIS band (Fig. 1. blue lines). The VIS-OCT uses a supercontinuum laser (SC) source (EXB-6, SuperK EXTREME, NKT Photonics, Denmark) equipped with a variable band-pass filter (SuperK Varia, NKT Photonics). The filtered output light (center wavelength: 480 nm, bandwidth: 20 nm, 80 MHz pulse rate) is delivered though a fiber delivery module. The VIS light is coupled into the source arm of a single-mode optical fiber-based Michelson interferometer. The NIR-OCT uses a superluminescent diode (SLD-37-HP, center wavelength: 840 nm, bandwidth: 50 nm, Superlum, Russia). After passing through an optical fiber isolator, the NIR light is coupled into another single-mode fiber-based Michaelson interferometer. The visible and NIR light beams, after exiting their corresponding optical fibers in the sample arms, are collimated and

Biomedical Optics EXPRESS

combined by using two dichroic mirrors (DM1: NT43-955, Edmund Optics and DM2: DMLP505, Thorlabs). The combined light beam is scanned by a x-y galvanometer (6215H, Cambridge) scanner, and delivered into the eye by the combination of a relay lens (L1, f = 75 mm, achromatic) and an ocular lens (L2, f = 20 mm, achromatic). The VIS light power was 500 μW before entering the eye, while the NIR light at the same location was 600 μW.

In the detection arm of each OCT subsystem, the reflected light from the sample and reference arms is collimated and detected by a spectrometer (SPEC1-2). The VIS-OCT spectrometer has an 1800 lines/mm transmission grating, a multi-element imaging lens (f = 150 mm), and a line scan CCD camera (Aviiva-SM2-CL-2010, 2048 pixels with 10 μm pixel size operating in 12-bit mode, e2V). The NIR-OCT uses a spectrometer with the same parameters as described in our previous publications [17].

The system for AF detection is similar to that described in our previous publications [13]. In short, the back-traveling fluorescent photons emitted from the fluorophore pass through the two dichroic mirrors and a long-pass filter (FGL515M, cut-on wavelength: 515 nm, Thorlabs), and are then focused into a 25 μm pinhole by an achromatic doublet with a focal length of 30 mm (L3). The AF photons are detected by a PMT module (PMM02, Thorlabs). The outputs of the PMT are digitized by a multifunction data acquisition board (DAQ, PCIe-6361, National Instruments) at a sampling rate of 2M/s. At each scanning position on the retina a total of 80 points corresponding to a sampling length of 30 μs were acquired. The amplitudes of the AF signal of these 80 points were averaged to form a single pixel of the AF image. Synchronization of the AF data acquisition, scanning of the galvanometer scanner and the OCT image acquisition was controlled by the multifunction DAQ board.

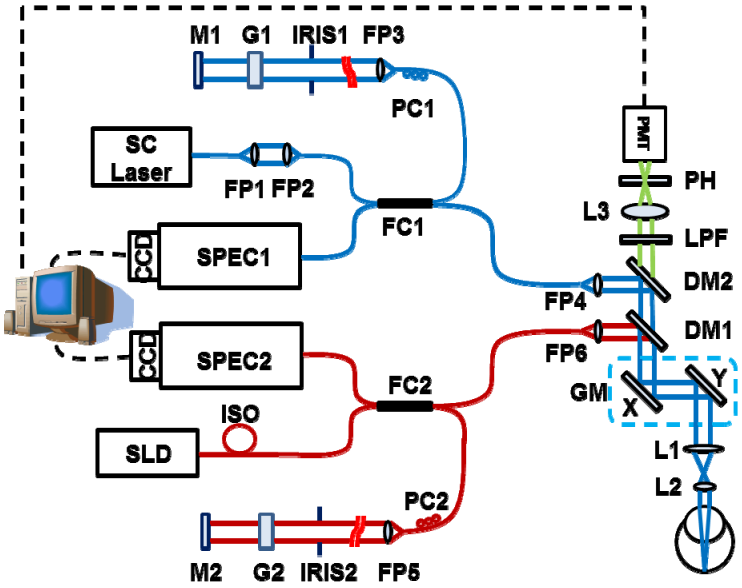

Fig. 1. Schematic of the imaging system. SC: supercontinuum; SLD: superluminescent diode; DM1-2: dichroic mirror; L1-3: Achromatic lens; LPF: long-pass filter; PH: pinhole; FP1-7: Fiber collimating port; ISO: Isolator; FC1-2: 3dB fiber coupler; PC1-2: Polarization controller; G1-2: BK-7 glass plate; M1-2: Mirror; IRIS1-2: Iris.

2.2 Modeling of OCT and AF signals of the retina

The light propagations in the retina were studied by many research groups. With reference to the model of fundus reflection proposed by van de Kraats et al [18,19], the measured light reflected from the retina can be divided into reflections from three sources, or three distinct layers of the eye. The first layer is the media anterior to the RPE. The second one is the RPE

Biomedical Optics EXPRESS

layer, where reflection by the RPE layer and absorption by the lipofuscin granules occurs. The third is the post-RPE layer, including the choroid and sclera. The intensity of the reflected light from pre- and the RPE layer can be expressed as:

$$I_{pre} = I_0.\tau_{pre}(\lambda)^2.R_{pre}(\lambda) \quad (1)$$

$$I_{RPE} = I_0.\tau_{pre}(\lambda)^2.\left[1-R_{pre}(\lambda)\right]^2.\tau_{RPE}(\lambda)^2.R_{RPE}(\lambda) \quad (2)$$

where I_0 is the light intensity incident into the eye, I_{pre} and I_{RPE} are the light intensities reflected from the pre-RPE and RPE layer, respectively; τ_{pre} and τ_{RPE} are the transmittance of the pre-RPE and RPE layer, respectively; R_{pre} and R_{RPE} are the reflectance of the pre-RPE and RPE layer, respectively.

The lipofuscin fluorescence intensity ($I_{AF\text{-}RPE}$) detected can be expressed as:

$$I_{AF-RPE} = I_0.\tau_{pre}(\lambda)^2.\left[1-R_{pre}(\lambda)\right]^2.\varepsilon.C.d.Q.A_d \quad (3)$$

where ε is the extinction coefficient of the fluorescent pigment (lipofuscin), C is the lipofuscin concentration, d is the RPE layer thickness, Q is the quantum yields of the fluorescence, A_d is the detecting efficiency including the detection solid angle, the response of the PMT, the gain of the circuitry, and the digitization coefficient.

Assuming that τ_{pre} and R_{pre} are the same for excitation light and the fluorescent, the ratio of AF and OCT signal is

$$\frac{I_{AF}}{I_{RPE}} = \frac{\varepsilon.C.d.Q.Ad}{\tau_{RPE}^2(\lambda).R_{RPE}(\lambda)} \quad (4)$$

In Eq. (4), all the parameters related to the incident light intensity and the transmission of all the eye components anterior to the RPE layer are eliminated.

2.3 Animal experiments

To test the capabilities of the imaging technique, we imaged the retina of albino Sprague Dawley rats (SD rats, Taconic). All the experiments were performed in compliance with the ARVO Statement for the Use of Animals in Ophthalmic and Vision Research and with the guidelines of the Florida International University's Institutional Animal Care and Use Committee.

The animals were anesthetized by intraperitoneal injection of a cocktail containing ketamine (54 mg/kg body weight) and xylazine (6mg/kg body weight). The pupil was dilated with 10% phenylephrine solution. Drops of artificial tear were applied during the imaging to prevent cornea dehydration and cataract formation. The rat was restrained in an animal mount, which was placed in a five-axis platform.

For FA imaging, Fluorescite 10% (100mg/ml fluorescein, 50mg/kg body weight) was injected though the tail vein after the rat was stabilized and the eye was aligned with the probe light. Then the simultaneous images were captured.

2.4 Phantom construction

To further test the imaging system and the theoretical models, we built a phantom to simulate light attenuation by tissues anterior to the RPE (Fig. 2(a)). The phantom consisted of three components: a plastic weighing dish as the container, fluorescein sodium solution in the container to simulate lipofuscin, and a transparent polystyrene membrane to cover the fluorescent dye solution and control the thickness of the sample. A set of ND filters (nominal OD values of 0.1- 0.5) was placed in front of the phantom for light attenuation.

Biomedical Optics EXPRESS

3. Results

3.1 Phantom test

We built a phantom to obtain proof-of-concept of the system design and theoretical models using ND filter to simulate signal attenuation. The phantom setup has two boundaries in the OCT cross sectional image: the 1st is the polystyrene membrane and the 2nd is the surface of the weighing dish. OCT and fluorescent images were simultaneously acquired. The OD value of the sample was measured to be 1.26 ± 0.02. By segmentation we obtained the intensity of the OCT reflection from the 2nd boundary (Fig. 2, red curve). As the OD value increases, both the fluorescent (Fig. 2(b), blue curve) and OCT signals decreased. But the normalized fluorescent signals (Fig. 2(b), Fluorescence/OCT, green curve) calculated using Eq. (4) showed only a gradual and linear decrease, which was caused by accumulated bleaching of the dye during the measurements as the measurements were taken sequentially from low to high OD values. Each measurement causes partial bleaching of the dye and the effect accumulates unless the time interval among measurements was sufficient for the dye to recover. It is clear that the normalized AF signals are independent of the OD values of the ND filter. As we noticed, the OD = 0.3 filter had a large deviation from the nominal OD value, which made the measured AF and OCT signal curves "non-linear" (Fig. 2(b), red and blue curves), and yet the linearity of the normalized AF curve was not affected (Fig. 2, green curves).

Results of these experiments demonstrated that OCT signals can be used as an internal reference to minimize the effects of media anterior to the RPE, and the imaging system functions as expected.

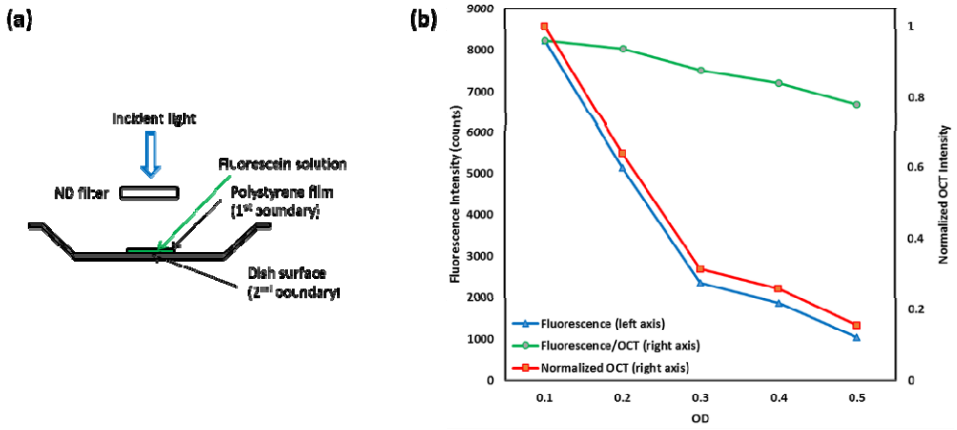

Fig. 2. Phantom simulation experiment. (a) Schematic of the phantom; (b) The AF/OCT (the AF intensity divided by the 2nd boundary OCT intensity, green) signals were not influence by the OD values of the ND filter, unlike the raw AF signals (blue) and OCT signals (red). The linear decrease of AF/OCT was due to accumulated bleaching of the dye.

3.2 in vivo simultaneous VIS-OCT and retina AF imaging

The system was tested in SD rats. Figure 3 shows an example of the simultaneously acquired VIS-OCT (Fig. 3(a) and 3(c)) and AF (Fig. 3(b)) images of the retina of an animal (age: 12 months; body weight: 500 g). Figure 3(a) is the projected OCT fundus image generated from the acquired 3D VIS-OCT data set [20]. Figure 3(c) is the VIS-OCT cross-sectional B-scan image, the location of which is marked as a dotted line in Fig. 3(a) and 3(b). The OCT data set consists of 512 (horizontal) × 128 (vertical) A-scans. Since the OCT and AF images are generated from the same photons we can see that Fig. 3(a) and 3(b) are precisely registered.

Biomedical Optics EXPRESS

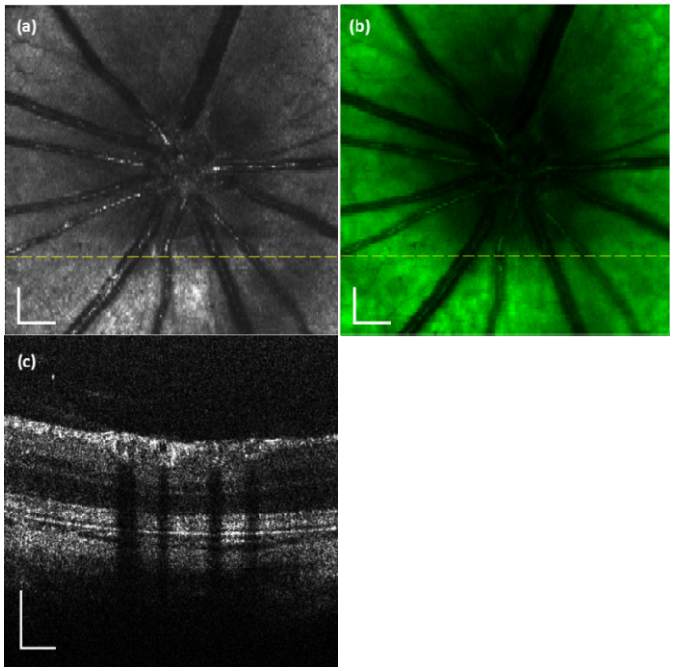

Fig. 3. VIS-OCT and AF images simultaneously acquired from a rat retina in vivo. (a) OCT fundus image; (b) AF image; (c) OCT B-scan image. The dotted line in the OCT fundus image marks the location of the OCT B-scan image. Bar: 200 μm

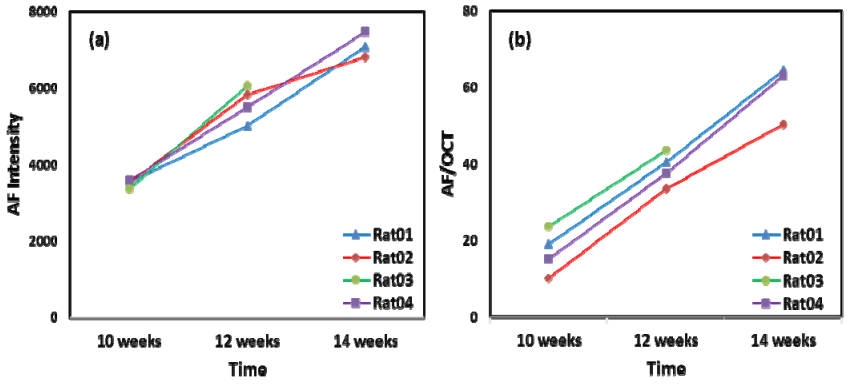

Fig. 4. The original AF intensities (a) and the normalized AF intensities (b) of four rats followed for a period of four weeks. Normalization was performed using the RPE image intensities calculated from the segmented OCT images.

In our previous studies [13], 4 SD rats (10-week-old) were imaged every two weeks (one rat died after the second imaging) to monitor their AF in the retinas for 4 weeks. The imaging conditions, including the focusing and the power of the probe light, the position of the reference arm, and the depth of the retina in the OCT image, were kept the same in each imaging experiment. The mean AF intensity counts over the entire imaged area of the 4 rats at different time points are shown in Fig. 4(a). The accumulation of lipofuscin in the RPE cells was evidenced by the increased AF image intensities over time.

The mean AF intensity counts were then normalized with the RPE OCT signal intensities obtained by manually segmenting the RPE layer and averaged over the entire imaged area. The normalized AF intensity is calculated by using Eq. (4). From the raw mean AF intensity counts, we can see significant increases over the 4-week period, but the rate of increase in

Biomedical Optics EXPRESS

each animal differs significantly. When the normalized data were used (Fig. 4(b)), the rates of increase among animals are quite similar. Note that the "levels" of I_{AF} in Fig. 4(b) between animals are not normalized to a common reference, and thus they cannot be compared quantitatively if not all the imaging conditions including the eye conditions are known. The Y axis scale in Fig. 4(b) has no specific physical meaning in this case.

All rats in the experiment were of the same age and housed under the same lighting conditions. It is reasonable to believe that the rate of lipofuscin accumulation is similar for all the rats. Before normalization using Eq. (4) the rate of AF intensity increase, thus the rate of lipofuscin accumulation, is significantly different among the different rats. After normalization using Eq. (4), the AF intensities of different rats increase over time at similar rate. Further, as we mentioned earlier, literature shows a linear correlation between aging and lipofuscin accumulation [21] which is better observed in the results using Eq. (4) for normalization.

3.3 in vivo simultaneous VIS-OCT and retinal FA

Since the system is capable of simultaneous OCT and AF imaging. We wondered if we can test this capability to image FA. Due to the relatively slow imaging speed, which is mainly limited by the bandwidth of the PMT and the line rate of the CCD camera used in the current system, we could not control which FA phase to capture. This limitation could be removed with a detector of higher speed to capture all the different FA phases.

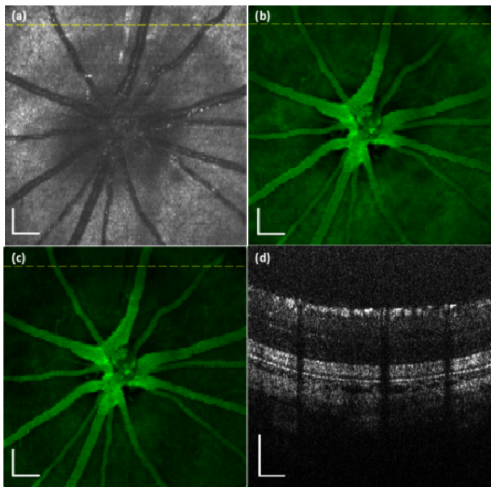

Fig. 5. VIS-OCT and AF images simultaneously acquired from a rat retina in vivo. (a) OCT fundus image; (b) AF image; (c) AF/OCT compensated fundus image; (d) OCT B-scan image. The dotted line in the OCT fundus image marks the location of the OCT B-scan image. Bar: 200 μm

The simultaneously acquired VIS-OCT and FA images of the retina of an SD rat are shown in Fig. 5. Spatial registration is guaranteed between the OCT and FA images because they were generated by the same photons. The FA image (Fig. 5(b)) was normalized with the projected OCT (Fig. 5(a)) intensities pixel by pixel (Fig. 5(c)) to produce better contrast for the retinal blood vessels. This contrast enhancement of the retinal blood vessels is achieved by suppression of the fluorescence signals from the choroidal blood vessels.

4. Discussion

We have demonstrated the capability of a multimodal imaging system for simultaneous OCT and fluorescent imaging with the same broadband light source. The fluorophores could be endogenous or exogenous. The major limitation for the current system is the imaging speed, which made the system unable to image the early FA phases.

Biomedical Optics EXPRESS

This system can be used to quantitatively imaging retinal AF, a measure of fluorophores mainly contained in the lipofuscin granules in the RPE [4,21]. AF was first detected in a vitreous fluorphotometry study [22]. The major fluorophore in lipofuscin granules and the major fluorophore of retinal AF is believed to be A2E (N-retinyl-N-retinylidene ethanolamine), a byproduct of the photoreceptor visual cycle [23–25]. The RPE is a monolayer of pigmented cells located between photoreceptors and the choroid [26]. It helps to enhance vision by absorbing scattered light with melanin, maintains the normal function of photoreceptors, including regenerating 11-cis retinal in the visual cycle [27] and phagocytosis of the shed photoreceptor outer segment tips [28]. Since lipofuscin has been implicated in retinal diseases such as AMD and Stargardt diseases, quantitatively measuring AF is of significant clinical value.

Quantification of absolute retinal AF intensities is important for AF to be used in clinical research and patient care, without which it is difficult to evaluate retinal AF images from different patients or even between successive images from the same patient. However, the available AF imaging technologies are not able to quantify absolute AF intensities. And this is the major hurdle for AF imaging to be widely utilized. We believe that to achieve quantification of absolute AF intensities, we need to have an internal reference to measure the true intensities occur at the RPE, and a fluorescent standard with known intensity as an external reference similar to the reference fluorescent target used by Delori and associates [15]. Our technique of simultaneous VIS-OCT and retinal AF imaging by using the same light source is unique in providing an internal reference to eliminate the attenuation effects of the media anterior to the RPE. Thus our system of simultaneous OCT and AF in combination with a fluorescent standard reference should be able to achieve quantification of absolute AF imaging for clinical application.

The system is also capable to simultaneously acquire OCT and FA images. For potential clinical application, the system will need faster detectors to capture different phases of FA. The multimodal VIS-OCT system described here is one of the several systems we have developed, including simultaneous photoacoustic microscopy (PAM) and autofluorescence microscopy [29,30], simultaneous OCT and PAM [31,32], and simultaneous OCT and retinal AF [12,13]. Further studies to optimize these systems in disease models could lead to clinical application these navel technologies.

To get the result of Eq. (4) we made an assumption that τ_{pre} and R_{pre} are the same for excitation light and the fluorescent. Although the assumption was made for simplifying the mathematical model, it is based on reasonable analysis. In the anterior segments light attenuation in the visible spectrum is mainly determined by the scattering coefficients of the tissues and light absorption can be ignored. Thus τ_{pre} is close to unity for the anterior segments. Light transmission is mainly determined by $(1-R_{pre})$, which slightly increases with wavelength in the visible spectrum [33]. For the retinal tissues anterior to the RPE, light absorption is mainly caused by hemoglobin in the retinal blood vessels, whose overall absorption coefficient increases with wavelength in the spectral range from 480nm to 570nm. In the meantime in the same spectral range light scattering decreases with wavelength. As a result, the overall effect of the ocular tissues anterior to the RPE layer $(1-R_{pre}).\tau_{pre}$ may remain relatively constant for the excitation and AF light. In future studies we will design experiments to test the accuracy of this assumption and improve the model if systematic error is introduced by the assumption. In addition, AF imaging is usually performed under light condition, so the effect of absorption spectrum by the visual pigment can be ignored.

In the phantom study, higher dye concentration will reduce the signal intensity from the second boundary. When the concentration of the dye is higher than a certain level, determined by the sensitivity of the OCT, the second boundary of the phantom could no longer be reliably imaged. In such an extreme situation, the normalization method cannot be used. We recognize that there are limitations of the current method. It seems unlikely that the limitations would be an issue in practice as we haven't seen the situation in which the RPE

Biomedical Optics EXPRESS

layer cannot be revealed in our in vivo imaging experiments on both albino and pigmented rats.

For in vivo imaging applications τ_{RPE} and R_{RPE} are functions of the concentrations of both melanin and lipofuscin in the RPE layer. Lipofuscin and melanin exist in the RPE cells as granules. Thus, the increase of lipofuscin will reduce τ_{RPE} but will increase R_{RPE} Lipofuscin accumulates during aging, but melanin will probably decrease [34] and the decrease in melanin would contribute inversely to τ_{RPE} and R_{RPE} How these combined effects influence τ_{RPE} and R_{RPE} cannot be easily answered and needs further investigation.

The normalization method is designed to remove the attenuation effects of the tissues anterior to the RPE layer as well as the effects of factors like misalignment, and to retain only the factors describing the optical properties of the RPE. Experiments with phantoms and in vivo studies on rats have demonstrated the promising potentials of the method to reach this goal. However, more specifically designed experiments are needed to examine the exact meanings of the method and its capabilities and limitations in extracting the true AF intensities of the RPE lipofuscin.

5. Conclusion

In conclusion, we have, for the first time, achieved simultaneous VIS-OCT and fluorescence imaging with a single broadband light source targeting both endogenous and exogenous fluorophores. This multimodal imaging system takes a significant step toward quantification of true retinal AF intensities. Further optimizing this system would make it as a valuable tool for clinical and research applications.

Funding

National Institutes of Health (NIH) (5R01EY019951).